On the use of LDV measurements for *in-vitro* aerosol deposition studies

Pedro J. Mendes[1,2], João F. Pinto[2], João M. M. Sousa[1]

1: Instituto Superior Técnico, Mechanical Engineering Dept., Av. Rovisco Pais, 1049-001 Lisboa, Portugal,
Email: pjmendes@navier.ist.utl.pt, msousa@alfa.ist.utl.pt
2: Faculdade de Farmácia, Pharmaceutical Technology Dept., Av. Prof. Gama Pinto, 1649-003 Lisboa, Portugal,
Email: pjmendes@ff.ul.pt, jpinto@ff.ul.pt

Abstract The turbulent flow inside a Twin Impinger (TI) has been characterized using a two-component fiberoptic Laser-Doppler Velocimeter (LDV) operated in backward-scatter mode. The principal aim of this work is to provide a better understanding of the aerosols' particles deposition process, thus helping the development of new particle formulations with optimal aerodynamic shapes and sizes, and ultimately promoting the deposition in the alveoli with improved therapeutic outcome. The standard TI is constructed in DURAN® glass and presents highly curved surfaces. Such characteristics lead to the requirement of applying a procedure for refractive index matching in the course of the LDV measurements, which precludes the possibility of using air as the working fluid. Usable fluids exhibiting the required value of the refractive index usually present a high viscosity, thus demanding large pumping power and leading to significant heat generation. For this reason, in a preliminary phase, water has been employed to minimize lens effects. Subsequently, exact refractive index matching has been achieved by the use of a special fluid in a thermostatic bath, but this introduced limitations on the range of investigated flow rates. Consequently, a critical assessment of errors had to be made in order to understand the implications of imperfect refractive index matching on the velocity measurements, namely in the vicinity of the walls. Dynamical similarity with air was prescribed throughout the experiments. Unfortunately this constraint cannot be met simultaneously for the particulate phase and therefore only information pertaining to the mean and turbulent flow fields of the continuous phase was gathered by laser-optic techniques. It was concluded that the flow inside the TI displays high complexity, thus major difficulties in turbulence modeling may be anticipated. The study has demonstrated that the coupled use of LDV and stochastic Lagrangian tracking can be used to reproduce particle deposition inside a TI, thus these results may be correlated also with particle deposition in the human respiratory tract.

1. Introduction

Delivery of drugs to the lungs as an aerosol is regarded as an excellent route for local or systemic applications due to the high therapeutical efficacy and acceptability by both patients and physicians. Aerosols have been used traditionally on the treatment of illnesses of the lungs and the respiratory tract, such as asthma, but in recent years the pulmonary route has been shown as an interesting choice for the administration of proteins as well. For instance, an aerosol was recently licensed for insulin administration (U.S. FDA, 2006). Unfortunately only a small fraction of the dose administrated as an aerosol reaches the alveoli (less than 40%). This lack of efficiency is due to several factors, namely the morphology of the patient airways and its respiratory patterns, and the characteristics of the device employed to deliver the drug and the characteristics of the powder, [e.g. size (Gonda, 1992), shape and aerodynamic behavior of the particles (Kleinstreuer and Zhang, 2003)].

In practice, the design of new formulations and inhaler devices must be assisted by a series of *in-vitro* tests. Aiming to assess the quality of the aerosols, samples containing the drug are produced and evaluated in testing devices such as cascade impactors (e.g. Andersen multi-stage impactor), or multistage liquid impingers, (e.g. Twin Impinger). These devices have been designed to simulate the movement and place of deposition of the particles in the respiratory tract and their use is compulsory once the design, production and evaluation of an aerosol are considered (EP, 2004).

The use of the above-mentioned devices allows the technologist to correlate the site of deposition in the device to the location in the respiratory tract where the particles will be settling. These tests are costly and time-consuming, and thus, a better knowledge and understanding of the movement of the biphasic flow (air and pharmaceutical particles) inside the testing devices, will help on designing new particles and on predicting their deposition in the bronchial and pulmonary mucosa. A better understanding of the flow can be promoted by direct measurements in combination with the use of a numerical model that reflects and predicts the experimental observations, both *in-vitro* and *in-vivo*. Aiming to run the *in-vitro* experiments, a Twin Impinger (TI) can be used and the flow inside the device can be characterized in real time using techniques such as Laser Doppler Velocimetry (LDV) or Hot-wire Anemometry (Doebelin, 1990). The TI is a transparent device allowing the optical access to its inside and consequently enabling the use of an optical measurement technique (e.g. LDV) without requiring physical interaction with the flow.

In summary, a detailed knowledge of the aerodynamics of the TI is expected to provide a better understanding of the aerosols' particles deposition process, thus helping the development of new particle formulations with optimal aerodynamic shapes and sizes, and ultimately promoting the deposition in the alveoli with improved therapeutic outcome.

Inside the TI, the aerosol flow entails a continuous phase (the air) and a discrete phase (the airborne particles). The application of a laser-optic measurement technique obliged the use of a refractive index matching procedure, employing a liquid as working fluid instead. Dynamical similarity with air flow has been prescribed throughout the experiments but this constraint cannot be met simultaneously for continuous and particulate phases. Although these techniques (e.g. Phase-Doppler Anemometry) present several advantages on the characterization of two-phase flows, the direct measurement of the discrete phase was not possible in this case.

In the present work, the combined use of detailed LDV data from the mean and turbulent fields of the continuous phase and stochastic Lagrangian particle tracking is proposed for *in-vitro* deposition studies. This methodology implies one-way coupling between the two phases, but it is expected that using LDV measurements of the continuous phase instead of data from numerical simulations will minimize the uncertainty associated to the prediction of a complex recirculating flow, when turbulence modeling is considered. However, the proposed procedure presents a few pitfalls as well, particularly due to the sensitivity of the deposition process to the near-wall flow characteristics. A model based on van der Waals particle-wall interaction has been considered to account for the adhesion of particles. On the other hand, particle-particle interaction was neglected based on the assumption that the particles were already dispersed enough inside the TI.

2. Methods

2.1 Preliminary studies

Prior to the quantitative measurements, visualization tests of the flow inside the TI were performed to identify the critical regions in the flow and provide a preliminary view of the flow physics. These tests were performed by installing a cylindrical lens in front of a 5-W Ar-ion laser beam to produce a light sheet (approximately 2-mm thick) at the central plane of the TI. The observations were recorded as digital photographs and video. To obtain tracers for these tests, particles of Iriodin 100 Silberperl (Merck, Germany) were suspend in water. Once this preliminary evaluation was accomplished, the LDV measurements started.

2.2 LDV assemblage

The TI (Figure 1) is made of DURAN® glass (refractive index $n = 1.473$) and its components present highly curved surfaces, which imposes specific difficulties to the measurements. These

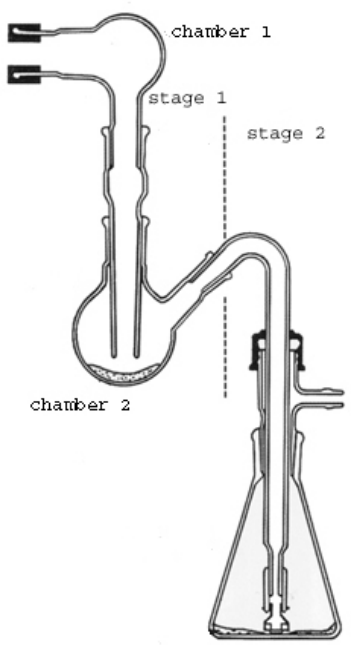

Figure 1 - Schematic representation of the Twin Impinger

problems were partially solved by submerging the TI in a liquid characterized by a refractive index close the above-mentioned value of n. The fluid chosen had to be pumped, to achieve dynamic similarity with the air (the fluid used in normal operation conditions of the TI), by imposing the same value of the Reynolds number. However, usable fluids exhibiting the demanded value of n usually present high viscosities, thus demanding high pumping power and leading to significant heat generation due to the viscous dissipation. To minimize these consequences, a compromise was initially found by using water as working fluid ($n = 1.337$ for $\lambda = 500$ nm). Subsequently, exact refractive index matching has been achieved by the use of a special fluid (weiβöl FC 2012 W, Fauth & Co, Germany) in a thermostatic bath, and a critical assessment of errors has been made, in order to quantify the implications of imperfect refractive index matching in the measurement of the velocity field (see Figure 2).

Pereira (1989) describes a methodology to quantify the aforementioned errors for cylindrical walls. The errors were evaluated at the location of four critical points (Figure 3) inside the first chamber of the TI: two of these points are in cylindrical zones (A and D); at the remaining points (B and C) two laser beams are aligned with the centre of the spherical chamber to measure the radial component of the velocity, thus responding to one of the curvatures of the sphere only, which makes it possible to consider the same procedure employed for cylindrical surfaces (Figure 2 b, case 1). The beams used in the measurement of the axial component suffer a deviation of the measuring control volume, due to the surface curvature, as shown in Figure 2a. However, the presence of the other curvature of the sphere may cause a displacement of the measurement control volume in the direction of the laser beams (case 2 in Figure 2b). These deviations will be added, enabling the view that the beams cross two cylindrical surfaces in different positions (perpendicular to each other). The first cylindrical surface has the diameter of the sphere (see Table 1) and the methodology to estimate the deviation of the control volume of the radial component of the velocity is used. The second surface has the diameter of the section of the sphere crossed by the plane containing the beams. In this case, the methodology to estimate the deviation of the control volume of the axial velocity component is used.

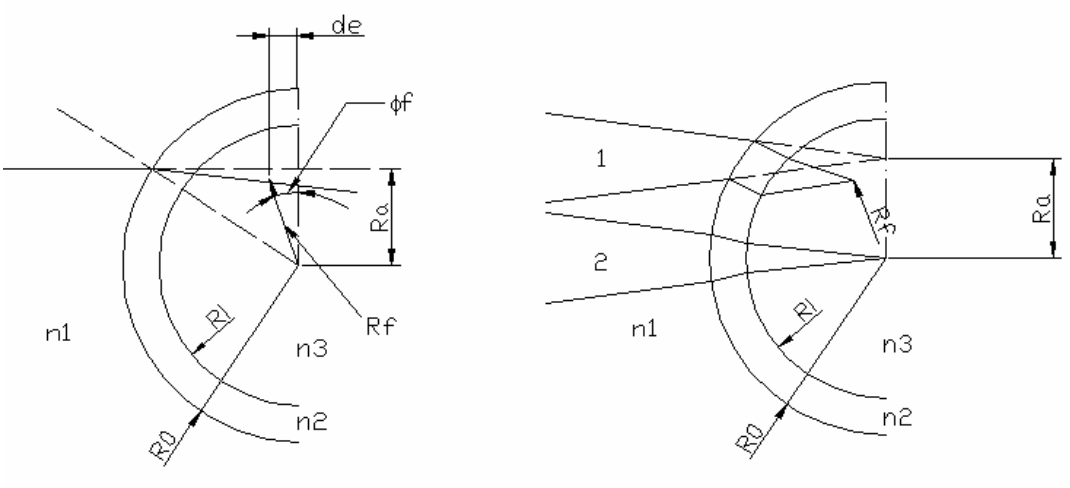

a b

Figure 2 - Schematics for the determination of the true position of the measurement control volume; axial (a) and radial (b) components of the velocity; $n1$, $n2$ and $n3$ - refractive indices

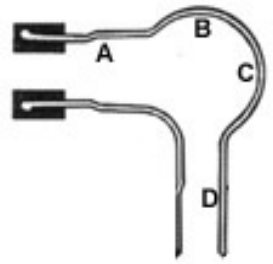

Figure 3 - The four critical points considered to evaluate the errors in the localization of the measuring control volume

Table 1 - Values of the relevant variables in each one of the critical points considered to estimate the errors

	A	B	C	D
Ri [mm]	13.5	23.9	23.9	8.7
R0 [mm]	14.5	24.9	24.9	9.7
*R*a [mm]	12.0	23.0	21.0	6.0

In the LDV measurements the mean flow field and the turbulent field were measured in five planes including the central plane. The flow rate of water was set to a constant value of 1.98 liters/min or 3.54 liters/min at a temperature of 25±1 ºC. These values are equivalent to a flow rate of approximately 30 liters/min or 60 liters/min of air through the TI. An air flow rate of 60 liters/min is the flow condition requested by the European Pharmacopoeia (2004) to test aerosols employing a TI. This value corresponds to the normal peak inspiratory flow rate of a healthy individual adult. On the other hand, the lower flow rate is associated to the inspiratory flow rates exhibited by children or asthmatic patients. The Reynolds number, based on the inlet diameter of the first stage of the TI and the corresponding velocity, were $1.6\mathbf{x}10^3$ and $2.8\mathbf{x}10^3$, respectively. The measurements at the higher water flow rate (3.54 liters/min) were also carried out to investigate the Reynolds number dependency in this range of operation. A comparison with the data obtained at 1.98 liters/min of water flow rate was performed, using normalized quantities based on the mean inlet velocity (U).

The velocity measurements were carried out employing a two-component fiberoptic LDV

system (Dantec, Denmark) operating in backward-scatter mode. Velocity statistics were computed by ensemble averaging from about $5x10^3$ or $7.5x10^3$ samples, for the lower or the higher flow rate, respectively. Nylon particles (5±1.5μm, Dantec) were used to obtain seeding.

Longer time series were also measured at 1.98 liters/min of water flow rate aiming to quantify the low-frequency flow oscillation identified in the top of the first chamber of the first stage of the TI during the visualization tests.

2.3 Stochastic particle tracking

The upper chamber of the TI (Figure 4) was discretized by a structured curvilinear mesh. The numerical mesh displays 32x32x70 nodes in *i*, *j* and *k* directions, respectively. A three-dimensional Eulerian model of the flow for the continuous phase was constructed from the detailed LDV data, under the assumption of axisymmetry. Lagrangian particle tracking was applied to the dispersed phase to identify the individual trajectories and deposition patterns of particles from pharmaceutical aerosols. A stochastic eddy-interaction model (Sommerfeld et al., 1993) has been used to account for the effects of turbulence in the tracking procedure. The planar mean flow velocities and the corresponding kinetic turbulence intensity in each one of the nodes of the numerical mesh were obtained by interpolation of the data from the LDV measurements, whereas the third velocity component was computed from the continuity concept (Sousa, 2002). A set of approximately $45x10^3$ computer-generated particles of lactose (density of 1.55 g/cm^3) with a diameter of 5±1μm, distributed according a Gaussian curve, was considered in the deposition study. Such characteristics constitute the first level of approximation to those exhibited by pharmaceutical drugs, delivered as an aerosol by Dry Powder Inhalers, in which lactose is used as carrier (Mendes et al., 2004).

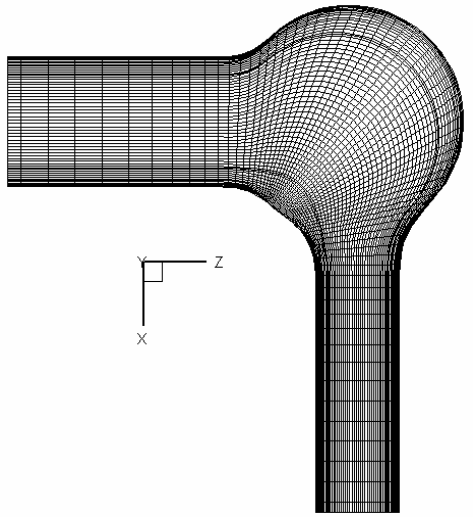

Figure 4 - Planar representation of the mesh used to simulate the first chamber of the first stage of the Twin Impinger

The numerical model developed to simulate the behavior of the particulate phase considers one-way interaction with both the air flow and the walls of the TI chamber. The forces acting on the computer-generated particles and affecting their movement are the inertial, drag, gravitational and virtual mass forces. Other mechanisms such as those resulting from Magnus, Saffman or Basset forces were not considered in this study because their relative importance was very small, when compared with the others (Chen, 1995). The impact of the particles to walls of the device was simulated by a restitution coefficient model (Chen and Pereira, 1997) and the particles were considered adhered to these walls when their kinetic energy after the impact was not sufficient to

compensate the van der Walls forces (Rimai and DeMejo, 1996). In the present work the Hamaker constant was set to 1×10^{-20} J.

3. Results

The visualization study portrayed an unstable flow, displaying significant dynamics of recirculation zones. In the first chamber, a recirculation zone in the top of the compartment and a stagnation area in the opposite side of the entrance can be observed (Figure 5a). From the top view of this chamber it is also possible to observe the occurrence of two recirculation zones on the sides of the compartment (Figure 5b). The dimension of these two regions was not constant in time and sometimes one of these zones occupied the entire chamber, which indicated the presence of low-frequency flow oscillations. The LDV measurements confirmed the existence of a low-frequency component in velocity time series taken in this chamber. The corresponding power spectrum displayed a dominant frequency (Figure 6) and allowed the quantification of the associated Strouhal number, $St \approx 0.02$.

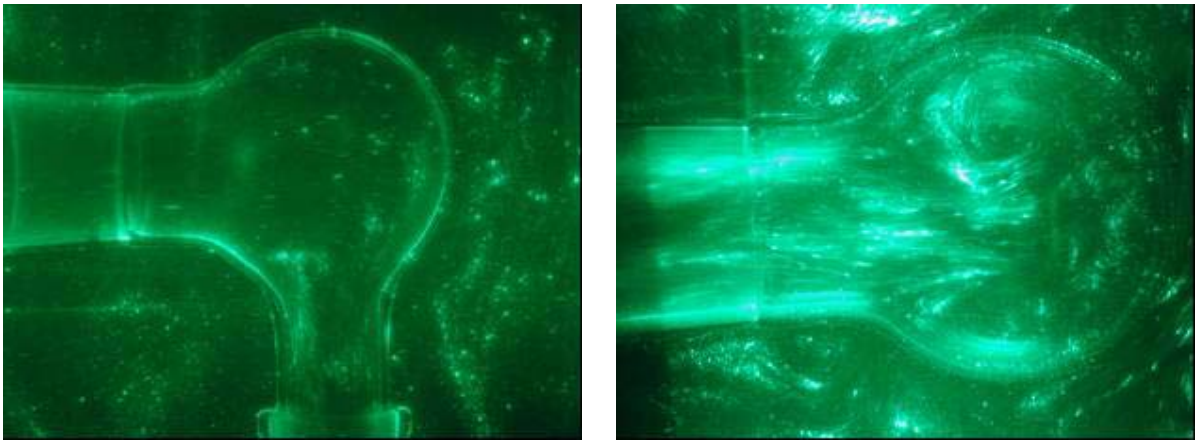

a) b)

Figure 5 - Flow visualization of the flow in the first chamber of the first stage of the Twin Impinger; a) front view; b) top view

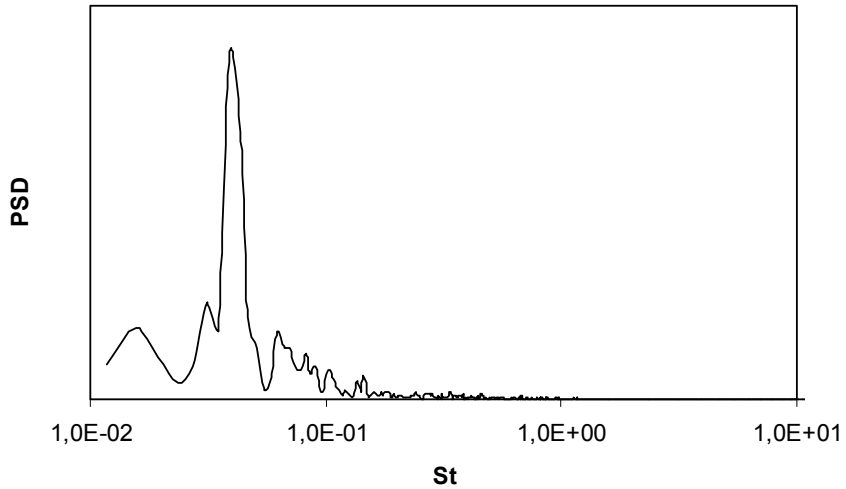

Figure 6 - Power spectrum of a velocity time series measured inside the first chamber

Inside the second chamber of the TI, an annular recirculation zone exists, which is confirmed by both front (Figure 7a) and side views (Figure 7b). This large structure in the flow wraps around the central tube connecting the first and the second chambers. A jet of high-speed flow can be seen exiting this tube (Figures 7a and 7b). The axisymmetry of the flow is destroyed by the connection to the second stage of the TI, observed in Figure 7a. By continuity, high velocities may be also expected in that area.

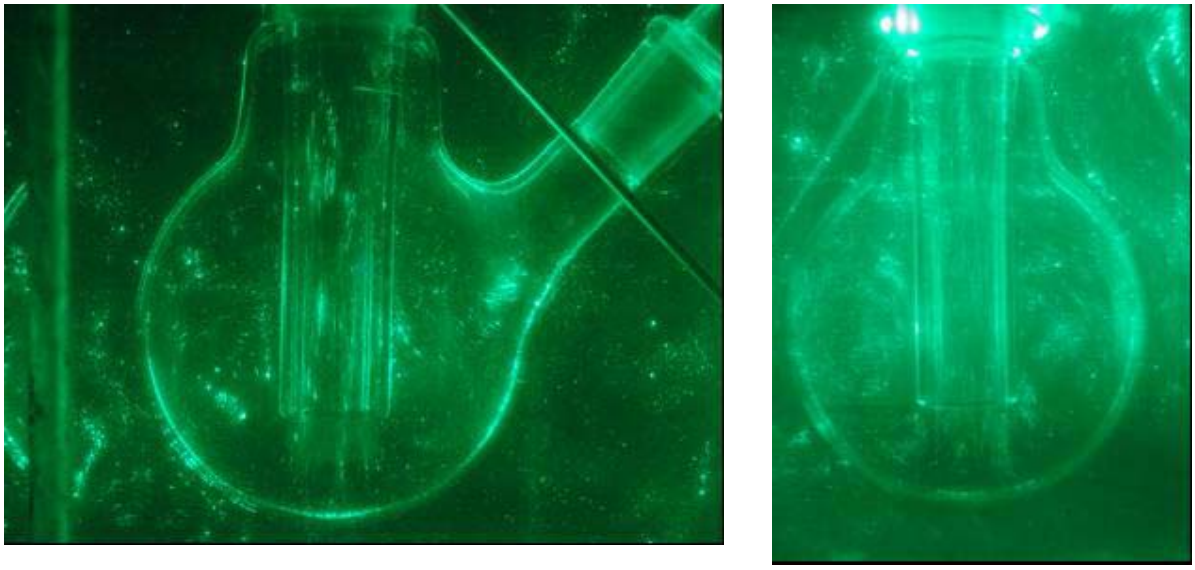

a) b)

Figure 7 - Flow visualization inside the second chamber of the first stage of the Twin Impinger; a) front view; b) side view

Some of the observations made during the flow visualization study were later confirmed by the LDV measurements, as shown in Figure 8. This figure presents the mean velocity field (shown by the vectors) and the turbulent kinetic energy field (shown by colored contours), for the lower (a and b) and the higher (c and d) flow rates, after normalization. In the mean flow field it is possible to identify again the recirculation and the stagnation zones. In the turbulent field, four different zones in the first chamber can be identified: the first characterized by low turbulence, at the entrance, the second overlapping the recirculation zone on the top of the chamber, the third displaying the higher turbulence values at the exit, and a forth zone at the center of the chamber. In the second chamber, the turbulence intensity is generally higher than in the first one and the regions showing larger values of turbulent kinetic energy are located in the vicinity of the bottom walls and at the exit of the chamber. These zones are always associated with regions displaying intense velocity gradients of the mean flow.

Figure 8 further allows a comparison between the two tested conditions (low and high flow rates). The data has been normalized and only the central plane of the TI is shown. There are minor differences in both mean and turbulent fields, mainly attributed to experimental uncertainty and repeatability difficulties. Very similar mean flow patterns can be observed in both situations, with the velocity vectors showing identical magnitude and orientation in each location. In the turbulent fields, identical patterns and magnitudes can also be identified, showing the same characteristic regions at both the lower and the higher flow rates. Thus, it may be concluded that there is a negligibly small Reynolds number dependency of the flow characteristics exhibited by the continuous phase in the investigated range of this parameter.

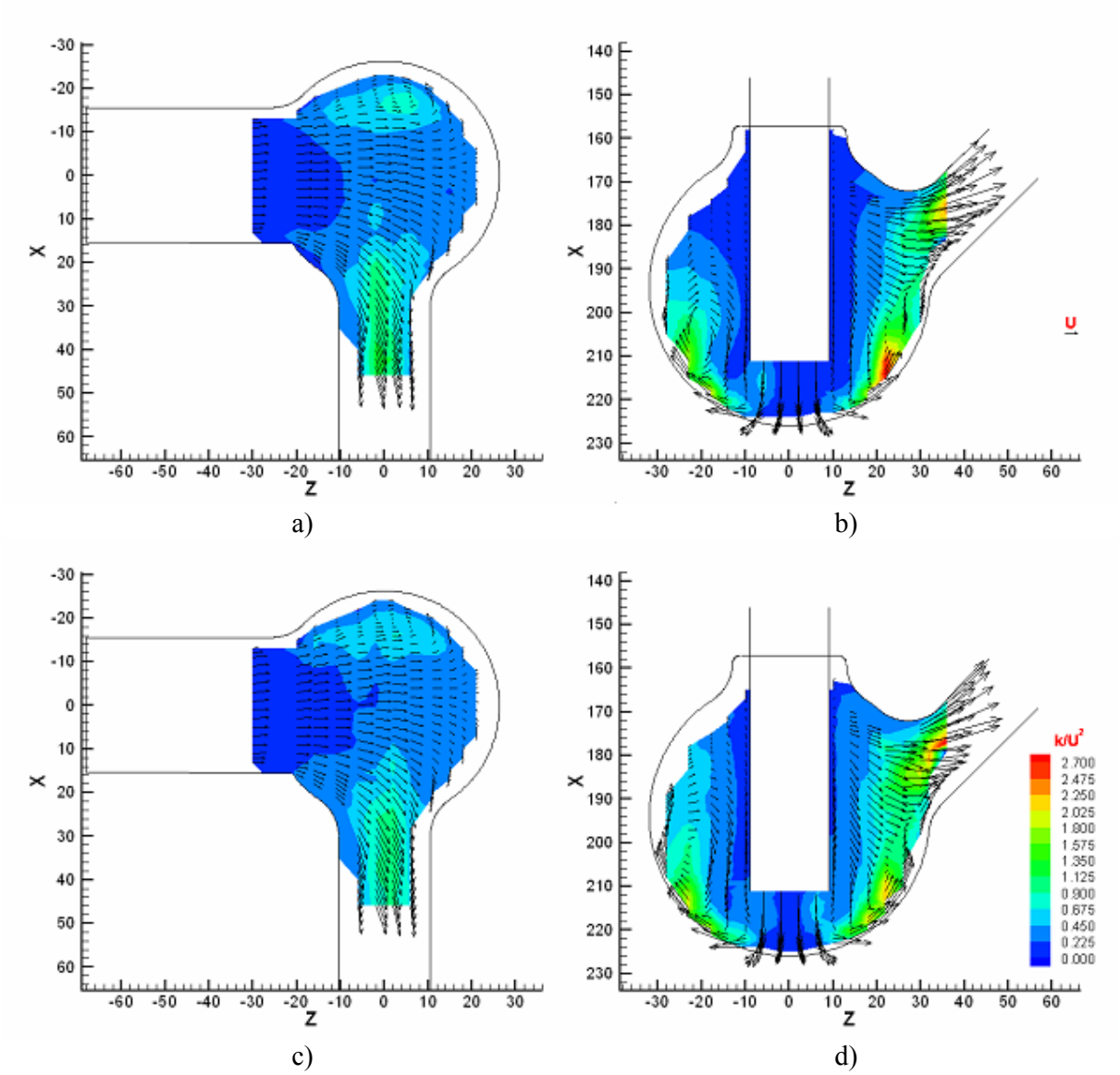

Figure 8 - LDV results of the normalized mean and turbulent fields for the two tested flow rates;
a) and b) lower flow rate; c) and d) higher flow rate;
a) and c) first chamber; b) and d) second chamber

The errors in the position of the control volume for the measurement of the velocity, due to the imperfect adjustment of the refractive index, are shown in the Tables 2 to 4. The meaning of the parameters shown in these Tables is explained in Figure 2. Table 2 shows the deviations suffered by the control volume used in the measurement of the radial velocity component. The distance between the centre to the position of the control volume (*Rf*) is identical to the expected value and the angle of the shunting line is very small (ϕf).

Table 2 - Errors in the position of the control volume of the radial velocity component for the characteristic points

	A	B	C	D
Rf [mm]	12.0	23.0	21.0	6.0
ϕf [rad]	$-3.19\text{x}10^{-02}$	$-5.04\text{x}10^{-02}$	$-1.85\text{x}10^{-02}$	$-1.42\text{x}10^{-02}$

Rf - distance between the centre to the position of the control volume; ϕf - angle of the shunting line

Table 3 shows the deviation of the control volume used in the measurement of the axial velocity component for the two considered points in the cylindrical regions (see Figure 3). The deviations (*de*) were very small (few micrometers) and the distances between the centre of the cylinders and the position of the volumes of control (*Rf*) were again similar to the expected values.

Table 3 - Errors in the position of the control volume of the axial velocity component for the two points in the cylindrical regions

	A	D
de [mm]	$-1.09\text{x}10^{-02}$	$2.13\text{x}10^{-02}$
Rf [mm]	12.0	6.0
ϕf [rad]	$-9.07\text{x}10^{-04}$	$3.55\text{x}10^{-03}$

de - deviation of the control volume from the central line; *Rf* - distance between the centre of the cylinder to the position of the control volume; ϕf - angle of the shunting line

The deviation of the control volume used in the measurement of the axial velocity component in points from the spherical zone, are shown in Table 4. As explained before, the deviations in these points can be seen as the addition of two separate deviations, associated to two different cylindrical walls. The two laser beams approach the wall with equal angles, but with opposite directions, thus the deviations compensate (Table 4, lower part) because the same media is present inside and outside the TI. The deviations caused by the other curvature of the sphere are again very small, for both of the points considered. The error in the position of these control volumes were only due to this second factor.

Table 4 - Values of the diameter of the section of the sphere and variables associated to it and the errors committed in the position of the control volume of the axial velocity component for the two points in the spherical region

		B	C
1st imaginary cylinder	*de* [mm]	$-4.05\text{x}10^{-02}$	$-1.14\text{x}10^{-02}$
	Rf [mm]	23.0	21.0
	ϕf [rad]	$-1.76\text{x}10^{-03}$	$-5.45\text{x}10^{-04}$
2nd imaginary cylinder	Diameter of the section of the sphere [mm]	13.0	22.8
	Ri [mm]	6.5	11.4
	R0 [mm]	7.5	12.4
	Ra [mm]	0	0
	Rf [mm]	0	0
	ϕf [mm]	0	0

de - deviation of the control volume from the central line; *Rf* - distance between the centre of the cylinder to the position of the control volume; ϕf - angle of the shunting line; *Ri* - internal radius and *R0* - external radius of the cylinder; *Ra* -distance between the centre of the cylinder and the entrance point of the beams, measured perpendicularly to these

By the use of the proposed three-dimensional reconstruction of the flow for the continuous phase described in the previous section, it was possible to provide a more complete representation of its features (Figure 9). In Figure 9a, which shows a top view of the mean velocity vector field, the two zones of recirculatory flow previously detected during the visualization tests can be observed. Figure 9b shows that the highest values of turbulence kinetic energy occur in the center of the vortices.

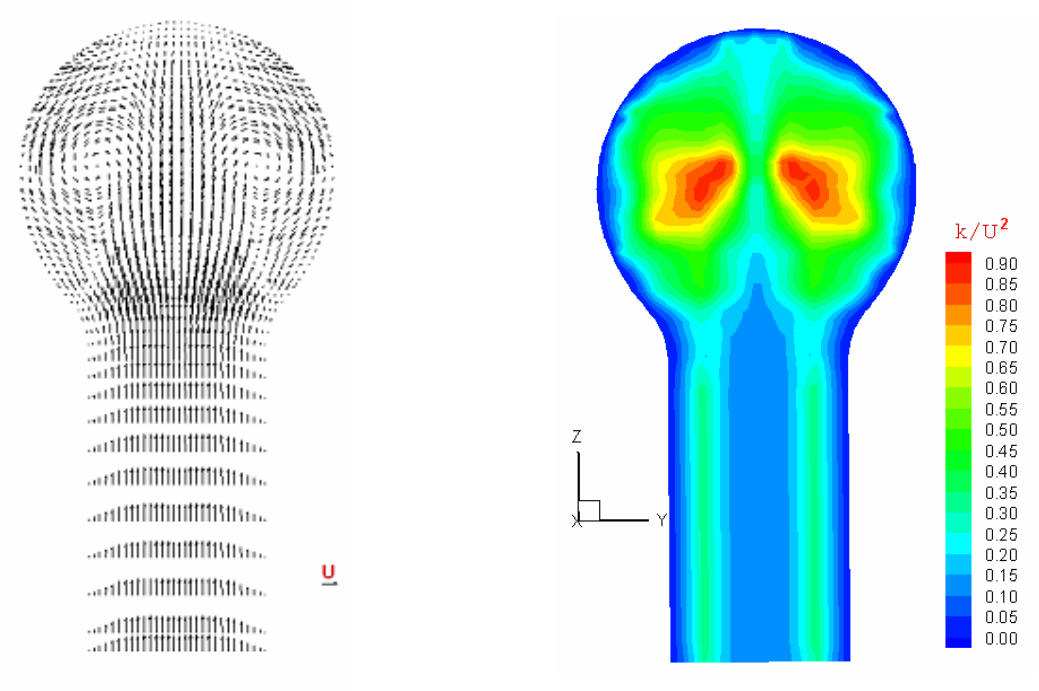

a) b)

Figure 9 - Top view of the three-dimensional flow model in the first chamber of the first stage of the Twin Impinger a) mean velocity field; b) turbulent field

The two vortices observed inside the chamber (Figure 9), together with the change on the direction of the mean streamlines, are responsible for the strong secondary flow occurring inside the tube connecting the first to the second chamber of the first stage of the TI (Figure 10). From the entrance (Figure 10a) to the exit (Figure 10b) of this tube, the centre of the Dean vortices moves slightly in *Z*-direction. However, the effect of turbulent diffusion is the most salient feature in this evolution.

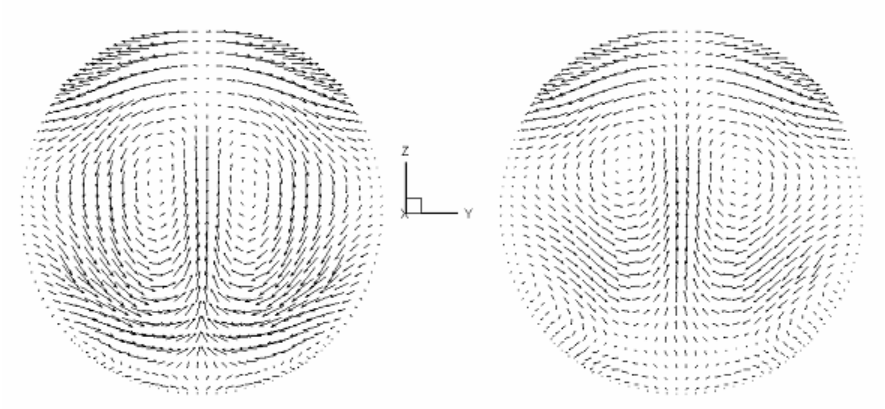

a) b)

Figure 10 - Secondary flow in the tube that connects the two chambers of the first stage of the twin impinger a) entrance of the tube b) exit of the tube

Figure 11 shows the pattern produced by the computer-generated particles, which have adhered to the walls of the device. The largest concentrations of particles can be observed at the bottom region located at the end of the inlet tube (A), on the wall at the opposing side of the entrance (B)

and at the entrance of the exit tube (C). In Figure 11b it is clearly seen the footprint of the particles at the exit tube, as a consequence of the secondary flow.

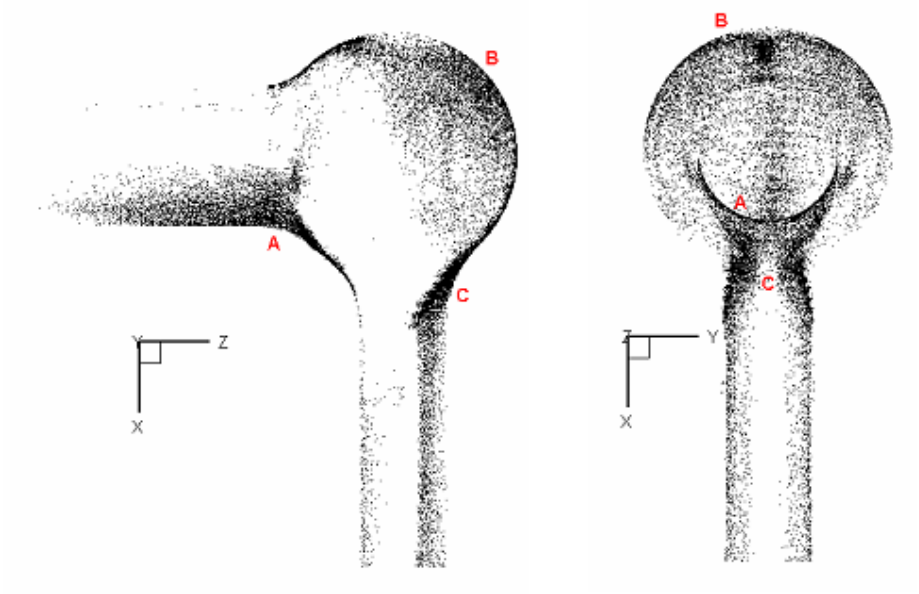

a) b)

Figure 11 - Deposition pattern of computer-generated particles in the first chamber of the Twin Impinger
a) side view; b) front view

4. Conclusions

The flow inside the Twin Impinger displays high complexity, including large-scale vortical structures, strong mean flow curvatures and flow oscillations, thus major difficulties in turbulence modeling may be anticipated.

Secondary flow develops is the tube connecting the two chambers of the first stage of the device, which affects the movement of the particles to the lower compartment.

A significant Reynolds number dependency was not observed affecting the mean and turbulent flow of the continuous phase, within the range defined by the inspiratory flow rates for normal adult and children/asthmatic patients.

The study has demonstrated that the coupled use of LDV and stochastic Lagrangian tracking can be used to reproduce particle deposition inside a TI.

As a consequence, a successful correlation of the results produced by the proposed methodology with particle deposition in the human respiratory tract may be expected as well.

5. Acknowledgements

This work was partially supported by the grants POCTI/EME/46902/02 and SFRH/BD/12124/2003 from *Fundação para a Ciência e a Tecnologia*, Portugal.

6. References

Chen X-Q, Pereira JCF (1997) Computational modelling of dilute gas-particle flows in an ultrasonic gas flowmeter. Flow Meas Instrum 8:167-182

Chen X-Q (1995) Numerical simulation of steady and unsteady two-phase spray flows. Ph.D. Thesis, Technical University of Lisbon, pp 29-32

Doebelin EO (1990) Measurement systems application and design. McGraw-Hill, Singapore, pp 527-608

European Pharmacopoeia (2004) European Directorate for the Quality of Medicines, 5th ed.

Gonda I (1992) Targeting by deposition. In: Hickey AJ (ed) Pharmaceutical inhalation aerosol technology. Marcel Dekker Inc, New York, pp 61-82

Kleinstreuer C, Zhang Z (2003) Laminar-to-turbulent fluid-particle flows in a human airway model. Int J Multiphase Flow 29:217-289

Mendes PJ, Raposo A, Sousa JMM, Pinto JF (2004) Sizing of powders in inhalers with Aerosizer according to a mixed experimental factorial design. J Aerosol Sci 35:509-527

Pereira JCF (1989) Refractive index matching for LDV measurements near wall and in complex geometries. In: Durão DFG et al. (eds) Instrumentation for combustion and flow in engines. NATO ASI Series E: Applied Sciences 154. Kluwer Academic Publishers, pp 267-284

Rimai DS, DeMejo LP (1996) Physical interactions affecting the adhesion of dry particles. Annu Rev Fluid Mech 26:21–41

Sommerfeld M, Kohnen G, Rüger M (1993) Some open questions and inconsistencies of Lagrangian particle dispersion models. In: Proc 9th Symp on Turbulent Shear Flows, Kyoto, Japan, 16-18 August, pap 15.1

Sousa JMM (2002) Turbulent flow around a surface-mounted obstacle using 2D-3C DPIV. Exp Fluids 33:854-862

US FDA (2006) FDA approves first ever inhaled insulin combination product for treatment of diabetes. Press release P06-13, January 27